

Inverse Imbalance Reconstruction in Rotordynamics

V. Dicken, P. Maaß, R. Ramlau *

C. Streller †A. Rienäcker ‡

November 18, 2003

Abstract

A method for identifying the distributed rotor imbalance from aircraft engine vibrations measured on the casing of the engine is presented. The problem is heavily ill-posed. Nonlinear regularization techniques for linear inverse problems and nonlinear functionals are suggested for stable reconstruction algorithms. ¹

Keywords: Rotor imbalance, inverse problem, whole engine model, vibration data analysis, continuous wavelet transform

MSC (1991) 65R30, 73D30, 73D50

1 Introduction

The goal of this work is to establish and compare algorithms for inverse imbalance reconstruction in aircraft turbines. Such algorithms are based on a validated whole engine model of a turbo engine under consideration. Based on the model, the impact of an imbalance distribution on the vibration behaviour of the turbine can be described as a matrix-vector multiplication $Af = g$, where f is the imbalance distribution and g

*Corresponding authors: Ronny Ramlau and Peter Maaß, Zentrum für Technomathematik, Universität Bremen, D-28344 Bremen, Germany, email: ramlau/pmaass@math.uni-bremen.de

†Carsten Streller, Rolls-Royce Germany GmbH, Eschenweg 11, D-15825 Dahlewitz

‡Adrian Rienäcker, MTU Aero Engines GmbH, Dachauer Str. 665 D-80995 München

¹The presented work was carried out as task of EU funded CERES consortium (cost effective rotordynamics engineering solution)

the vibration response. It turns out that the matrix A is very ill-conditioned. As the measured data is highly affected with noise, we have to use regularization methods in order to stabilize the inversion. Our main interest was in the use of nonlinear regularization methods, in particular *nonlinear filtered singular value decomposition* and *conjugate gradient* regularization.

1.1 Motivation

While weight reduction efforts in aeroengine design lead to flexible casing structures, sensitive to vibration excitation from the main rotors, the market demands the smallest possible level of vibrations transmitted to the aircraft, in order to maximize passenger comfort. This holds especially true for the market segment of long range business aircraft, where engines are generally mounted directly to the fuselage and low cabin noise and vibration levels are essential in meeting customer expectations. Lowering vibrations caused by imbalance in the rotating parts may also help to increase safety and lifespan of aircrafts through reducing material fatigue.

The BR700 family of aeroengines already incorporates key elements for low vibration levels - a stiff high pressure rotor design, squeeze film dampers on all bearings and tight balancing limits. In order to further improve aircraft comfort and quietness for business jets, a project with the task to minimize engine vibration levels was launched for BR710 right after engine certification. Since low pressure spool synchronous vibration levels can be reduced with standard trim balancing methods with relatively little effort and expense, project focus was on reducing vibrations excited by the imbalance distribution on the high pressure (HP) spool (compressor, turbine and related components). The HP shaft is not accessible after engine build, which enforces the principle of 'right first time' on balancing and assembly. With a certified design and approved balancing procedures, the main objective was to understand the system and to find the feasible changes in procedures and parts which help to improve product quality.

A direct measurement of HP vibrations in the assembled engine is impossible, due to narrow space, high forces and temperature, therefore we have to rely on indirect measurements. System response to imbalance excitation depends on the magnitude and distribution of the excitation itself, the transfer characteristics from rotor to stator and the amplification characteristics of the stator. Any attempt to minimize dynamic casing responses must consider all these parameters.



Figure 1: Gulfstream business jet BR 710 engine Engine interior

1.2 Available data

Let us start with a brief description of the measurement process and the necessary preprocessing of the raw data. It is relatively easy to measure vibrations on the casing of the engine using acceleration sensors. Using Fourier-transform or wavelet algorithms it is possible to separate signal components related to the fast rotating high pressure compartment and the slower low pressure system of the engine. Let us call $s(t)$ the raw signal component related to the first engine order of the high pressure compartment in the primary time series of acceleration data. This component is modeled as sample values of

$$s(t) = \alpha(t) \cos(i\omega(t)t + \phi(t)) + noise(t) .$$

It is assumed that - as long as the change in frequency of the engine is slow enough - the current amplitude satisfies

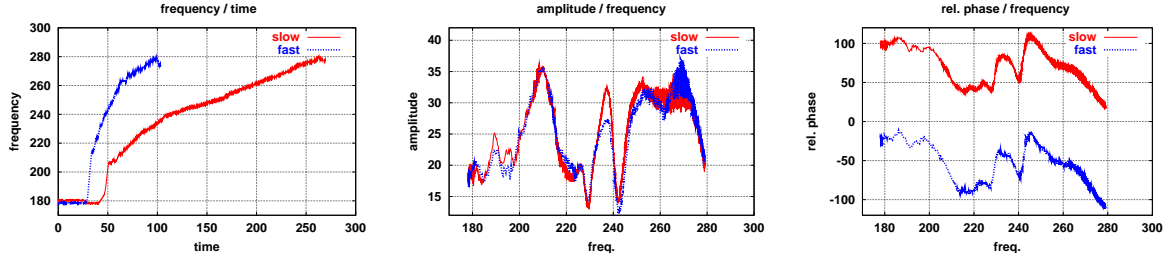
$$\alpha(t) = a(\omega(t))$$

and likewise the current phase shift

$$\phi(t) = p(\omega(t)) .$$

Here $a(\omega)$ and $p(\omega)$ denote the steady state amplitude and steady state phase shift of the engine running at constant frequency ω . The quantities $a(\omega)$ and $p(\omega)$ satisfy the mechanical laws of systems of coupled damped oscillators. From the available noisy sample values of $s(t)$ using FFT or wavelet techniques one can identify the current frequency $\omega(t)$ of the turbine and the amplitude $\alpha(t)$ of the vibration caused by imbalances in the high pressure compartment. The phase $\phi(t)$ can only be computed if a once per revolution signal is available.² If $\omega(t)$ is known from once-per-revolution signals, the amplitude $\alpha(t)$ and phase $\phi(t)$ can also be determined by computing discrete Fourier-transform coefficients or wavelet coefficients only for the current frequency.

² In the particular engines studied here the once per revolution signal is reconstructed from a once per revolution signal after a 73:20 gear-box, therefore only relative phase information can be obtained.



Freq. versus time

Amplitude versus Freq.

Phase versus Freq.

Figure 2: Raw data of frequency, amplitude and phase extracted from time sequence of acceleration data (one sensor, a slow and a fast idle to maximum cycle are shown).

The data of current frequency, instantaneous amplitude and instantaneous phase are gathered over an idle to maximum power cycle of the engine. The extracted data are assembled to form an irregularly spaced sampling of the complex valued vibration data

$$g(\omega) = a(\omega) \exp(i \cdot p(\omega)) ,$$

the steady state system response with amplitude $a(\omega)$ and phase $p(\omega)$, in the interval [150Hz-270Hz] for the engine type of interest. This operating range is well below the first rotor-critical resonance frequency of the engine.

The actual data $g^\varepsilon(\omega)$ are noisy, possibly multi-valued samples of $g(\omega)$ because of measurement errors and the transient measurement. Due to the later the system may not always have the time to attain the stable steady state equilibrium and e.g. show different amplitude values at the same frequency at different times. Figure 2 shows two sample data sets.

In some cases it is possible to use more then one sensor position during tests, which gives access to the corresponding number of system response functions at various locations on the casing.

1.3 Analysis of measured data

In order to use the available data in numerical algorithms for the reconstruction of the underlying imbalance distribution (called f in the sequel), we need to interpolate the data onto some regular grid and estimate their noise level. Figure 3 shows the average of two measurements obtained by interpolating to a regular 1/3 Hz grid the data collected during a slow and a fast idle to maximum power cycle of the engine (cf. Fig. 2). Further the distance of the measurements between each other resp. to the average is shown (absolute and relative) to estimate the quality of the measurement.

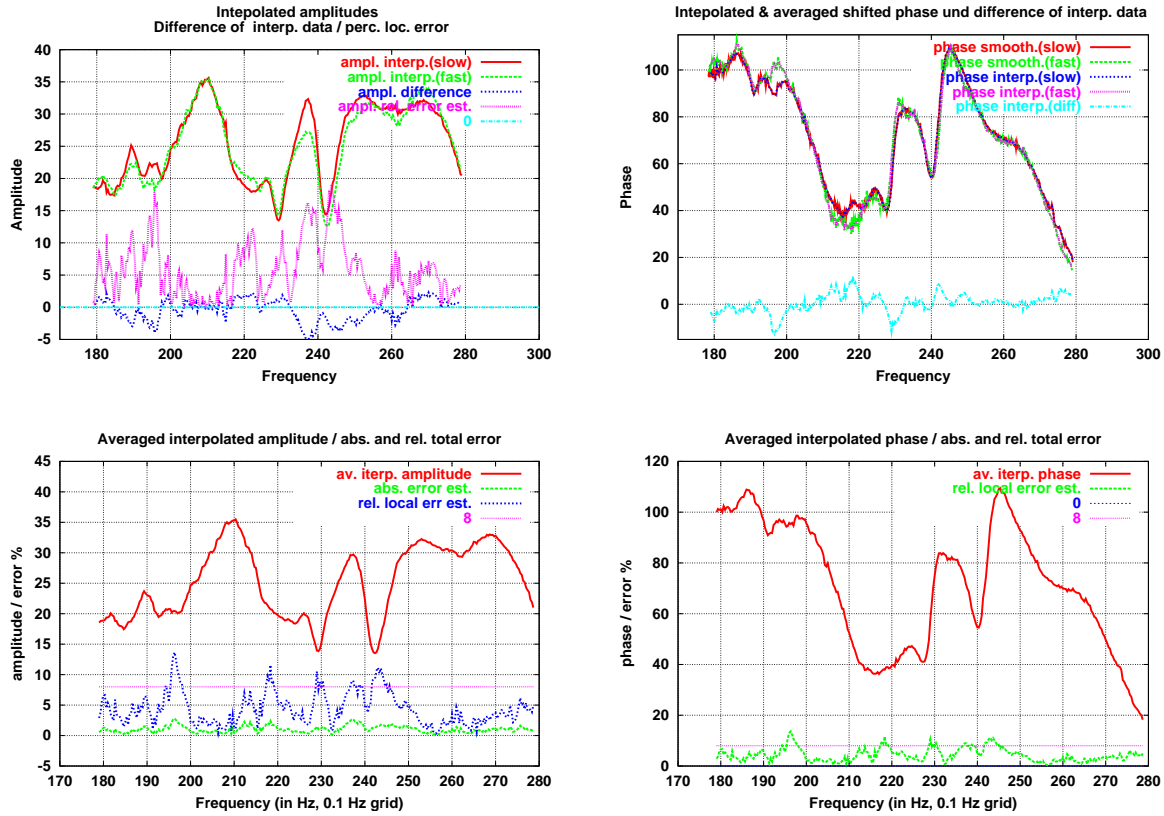


Figure 3: Extracted data interpolated to regular grids with error estimate

The relative phase information was reproduced up to 1.0% and the amplitude could be reproduced with an accuracy of about 5.4%. The relative total mean square error is estimated to be 4.5%. Herein the error estimate is defined as distance of either realization to the mean of both and is equivalent to a SNR of 13.5 dB.

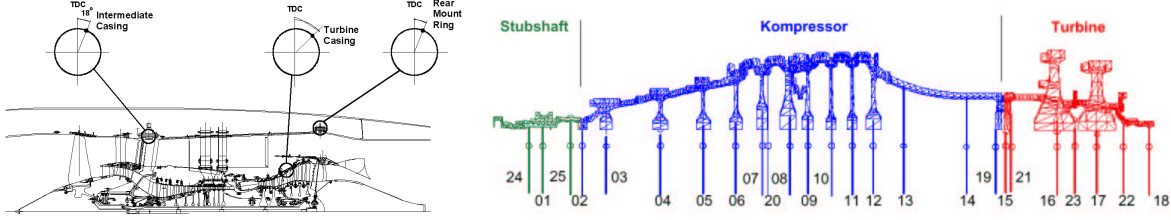


Figure 4: a) Casing vibration measurement location b) Imbalance locations considered

2 Mathematical model of vibration causes

First of all we assume that relevant contributions to the imbalance are concentrated only at few discrete locations (indexed by l) with high mass density in the high pressure system. The system response is assumed to be linear. This appears to be justified as long as the amplitude $a(\omega) = |g(\omega)|$ is small enough, such that the superposition principle can be applied. For large amplitudes the system response will be nonlinear due to nonlinear damping effects in the squeeze film dampers.

Assuming superposition is valid a distributed imbalance $f = (f_l)_{l=1}^L \in \mathbb{C}^L$ with weight $|f_l|$ under relative angle $\arg(f_l)$ at location l causes a system response vibration which has the form

$$g(\omega) = \sum_{l=1}^L g_l(\omega) f_l ,$$

where $g_l(\omega)$ is the system response to a unit imbalance at position l under angle 0. The mayor requirement to formulate the model is the existence of a validated whole engine model. Such a model was implemented at Rolls-Royce Germany in an elaborated finite element program (NASTRAN code). Therewith the contribution $g_l(\omega)$ of a unit point imbalance at any relevant location l can be computed on a regular sampling grid $\{\omega_k | k = 1, \dots, K\}$ in the frequency interval of interest. Relevant locations are possibly the positions of the bladed discs, the bearings and the joints in the high pressure rotor and further the centers of gravity of the rotor components (cf. Fig. 4). Thus if measurement and model were perfect the data $g := (g(\omega_k))_{k=1}^K$ should be given by $g = A \cdot f$ with the complex matrix $A = (a_{kl}) \in \mathbb{C}^{K \times L}$, $a_{kl} = g_l(\omega_k)$ for any imbalance $f = (f_l)_{l=1}^L$. In case multiple (N) sensors are used one has for each sensor j and each frequency ω_k the quantities $g^j(\omega_k)$, $j = 1, \dots, N$. For convenience the indices (k, j) , $k = 1, \dots, K$, $j = 1, \dots, N$ are replace by $k' = N \cdot (k - 1) + j$, $k' = 1, \dots, K' = N \cdot K$. The data then become $g_{k'} = g^j(\omega_k)$, $k' = 1, \dots, K' = N \cdot K$, ($j = k' \bmod N + N$, $k = [k'/N] + 1$). For simplicity we drop the $'$ and continue to write k and K also in the multiple sensor case (where double indices (k, l) should formally be used). Figure 5 illustrates the mechanical model and the finite element grid used in

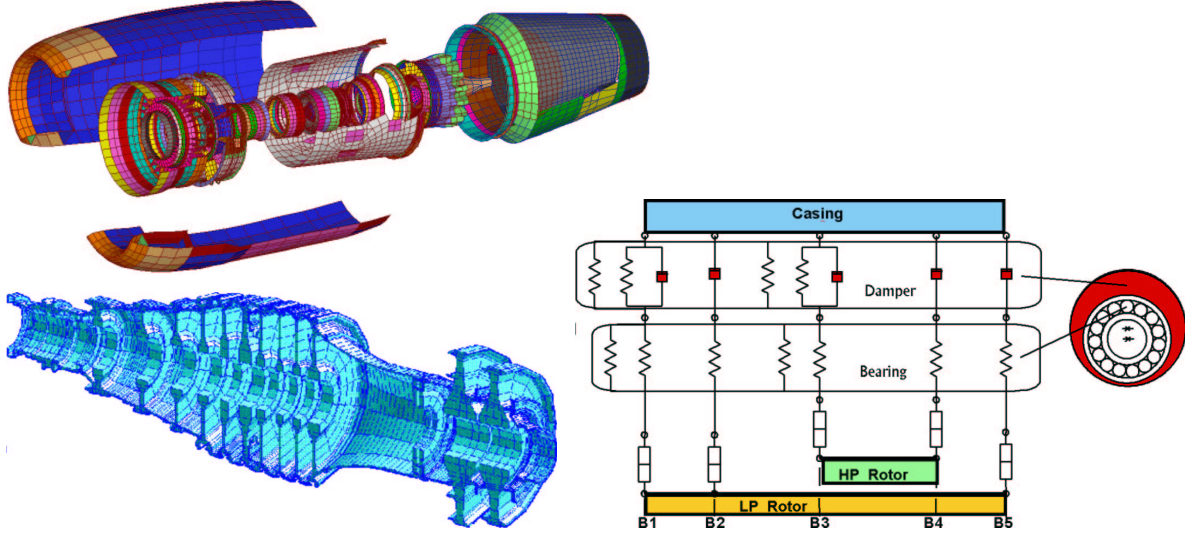


Figure 5: Whole Engine Model Finite Element Structure. The engines casing modules together (top) have about 110,000 FEM nodes with 450,000 degrees of freedom. For the HP rotor alone (bottom left) the NASTRAN FEM model uses 25,000 nodes with 76,000 degrees of freedom. The right figure shows the mechanical model with a squeeze film damper in some detail.

the whole engine model for the computation of the system matrix A .

2.1 Inverse Problem

Due to measurement variance and modeling error only noisy data

$$g^\varepsilon = A \cdot f + z$$

are available in real applications. The task is to recover f as good as possible from g^ε , using only our knowledge of A and relative error estimates like

$$\frac{\|z\|_2}{\|g\|_2} \leq \varepsilon \quad \text{or} \quad \mathbb{E}(\|z\|) \simeq \varepsilon \|g^\varepsilon\|.$$

This inverse problem of reconstructing f is difficult because the matrix $A \in \mathbb{C}^{K \times L}$ is very ill-conditioned. This can be seen from the singular value decomposition (SVD) of A . We assume sufficiently many frequencies and sensors were chosen, s.t. $K \geq L$. Then there exist orthonormal bases $U = (u_i)_{i=1}^L$ and $V = (v_i)_{i=1}^K$ with singular vectors $u_i \in \mathbb{C}^L$, $v_i \in \mathbb{C}^K$ and singular values $\sigma_i \geq \sigma_{i+1} \geq 0$ s.t.

$$v_i = \sigma_i A u_i \quad \text{and} \quad u_i = \sigma_i A^* v_i \quad \forall i = 1, \dots, L.$$

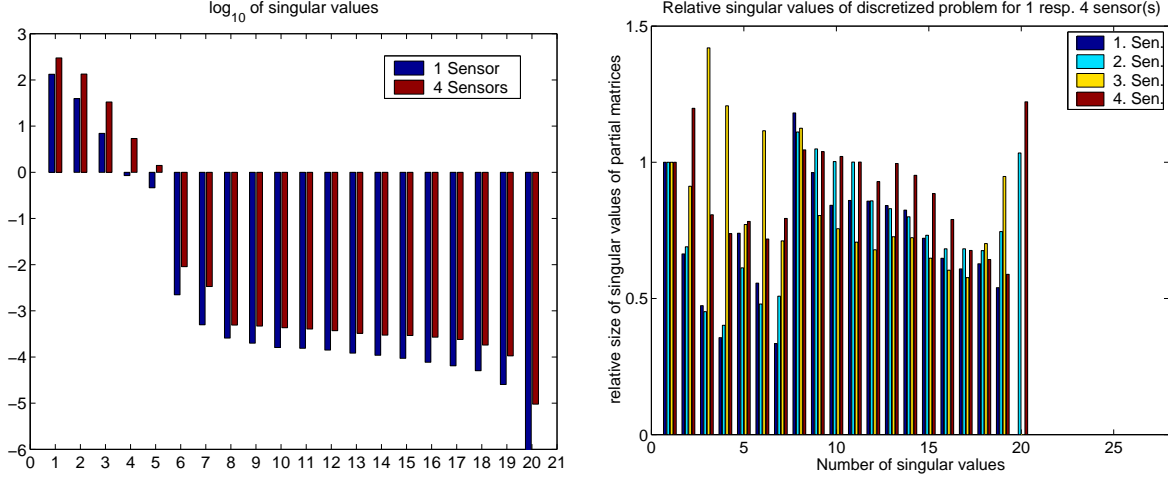


Figure 6: a) Distribution of singular values b) Relative condition numbers of partial data problems.

Further we set $\sigma_i = 0$ for $i > L$ and denote by Σ the $L \times K$ matrix whose only nonzero entries are the σ_i along the diagonal. Thus the matrix A can be decomposed as

$$A = V\Sigma U^*, \quad \text{i.e.} \quad Af = \sum_{i=0}^L \sigma_i \langle f | u_i \rangle v_i.$$

For the vectors v_i and u_i the eigenvalue equations $A^*Au_i = \sigma_i^2u_i$ and $AA^*v_i = \sigma_i^2v_i$ hold. Figure 6a) shows the distribution of the singular values σ_i for two discretizations obtained using one resp. four sensor positions. Here the frequency grid used with the whole engine model had a grid width of $\Delta\omega = \omega_{k+1} - \omega_k = 2\text{Hz}$, which leads to $K = 61$ resp. $K = 4 \cdot 61 = 244$ data points when 4 sensors are used. In our experiments $L = 20$ or $L = 25$ possible positions for imbalance locations were considered. If we anticipate a noise level ε of 1%-10% (SNR 10 – 20 dB), it can be seen that at most 5 singular values can directly be used for stable reconstructions. This corresponds to the engineering experience that five degrees of freedom are sufficient to model a rotor, even one with very complex geometry, at speeds in the undercritical range [GP75].

It might be somewhat surprising, that ignoring some of the data, i.e. selecting a properly chosen subset of the data may improve the condition of the task: We considered for the 4 sensor case partial data from just one of the sensors. Let us consider the subset of data from the j^{th} sensor and define matrices A^j with singular values σ_i^j that correspond to using only partial data from sensor j and A^* , σ_i^* related to the full information of all 4 sensors. We define as relative condition number for i singular values and the subset of data from the j^{th} sensor the quantities

$$c_{ij} := \frac{\sigma_i^j}{\sigma_i^*} \cdot \frac{\|A^*\|}{\|A^j\|} = \frac{\sigma_i^j}{\sigma_i^*} \cdot \frac{\sigma_1^*}{\sigma_1^j}.$$

In our case considering only data from sensor 3 leads to better condition numbers in particular for $i = 3, 4, 6$ than the full data as can be seen from Figure 6b. This is intuitively reasonable because sensor 3 is closest to the turbine and therefore may 'feel' the imbalance better. Yet it is not fully understood how using additional information from other sensors can, against intuition, really make the task more difficult. Probably using an optimized weighting over the sensor positions would yield the best condition numbers for the truncated problems. The question how to compute such a weighting remains open.

3 Regularization methods

3.1 Pseudo-inverse and Regularization

The formal inverse of the SVD of A , called generalized or pseudo inverse, is defined by

$$A^\dagger g := \sum_{\substack{i=0 \\ \sigma_i > 0}}^L \frac{1}{\sigma_i} \langle g | v_i \rangle u_i .$$

A numerical implementation of A^\dagger is very unstable or impossible, if some of the $\sigma_i > 0$ are some orders of magnitude smaller than $\|A\| = \sigma_1$. This is the case for the problem at hand, as can be seen in Figure 6a. Results of applying A^\dagger to g^ε would be dominated by amplified noise and rounding errors. Thus a stable regularization of A^\dagger is needed. Such a regularization can be represented as a filtered SVD (cf. [Lou89])

$$T_\gamma(g) := \sum_{\substack{i=0 \\ \sigma_i > 0}}^L \frac{w_{\gamma,i}(g)}{\sigma_i} \langle g | v_i \rangle u_i .$$

If all $\frac{w_{\gamma,i}(g)}{\sigma_i}$ are bounded by a number of moderate size, then the evaluation of T_γ is numerically stable. The task is to find suitable weights $w_{\gamma,i}(g)$ to balance noise amplification versus the regularization error introduced by choosing T_γ in place of A^\dagger . Usually T_γ is chosen from a family of regularization operators parameterized by a regularization parameter γ for which $\lim_{\gamma \rightarrow 0} T_\gamma(g) = A^\dagger g$ holds pointwise for all $g \in \mathcal{D}(A^\dagger)$. Once the family is chosen, the often nontrivial task remains to identify an optimal value of γ .

Let us consider noisy data $g^\varepsilon := Af + z$ and define $f_\gamma^\varepsilon := T_\gamma(g^\varepsilon)$. Further we denote the perfect data by $g = Af$ and define $f^\dagger = A^\dagger g$. The vector $f^\dagger \in \text{kernel}(A) + f$ represents the smallest imbalance distribution which would explain perfect data.

The question how to choose the weights $w_{\gamma,i}(g)$ and thus T_γ best arises immediately. A number of suggestions can be found in the literature (cf. [Lou89]). The classic approaches use linear filters, i.e. $w_{\gamma,i}(g) = w_{\gamma,i}$. If the singular vectors u_i and v_i can be computed (as in our problem) the truncated SVD first comes to mind. It uses $w_{\gamma,i} = 1$ if $\sigma_i \geq \gamma$ and $w_{\gamma,i} = 0$ otherwise.

In the mathematical community a regularization technique suggested by Tikhonov about 1962 is more popular. Tikhonov regularization employs

$$w_{\gamma,i}(g) = w_{\gamma,i} := \frac{\sigma_i^2}{\sigma_i^2 + \gamma} ,$$

but can be computed without knowledge of the singular vectors and values as

$$f_\gamma^\varepsilon = \operatorname{argmin}\{\|Af - g^\varepsilon\|_2^2 + \gamma\|f\|_2^2\} =: \operatorname{argmin} J_\gamma(f) .$$

In this form Tikhonov regularization extends to nonlinear inverse problems. Equivalently and numerically often it is computed as solution of $\nabla J_\gamma(f_\gamma^\varepsilon) := 0$, which in the linear case is equivalent to the normal equation

$$(A^*A + \gamma)f_\gamma^\varepsilon = A^*g^\varepsilon$$

derived from the vanishing gradient condition.

Both methods and other standard linear methods like Landwebers method are not optimal if the problem is as ill-conditioned as the one at hand and if the signal f to be reconstructed has significant components $\langle f | u_i \rangle$ for i corresponding to small singular values σ_i . Further the truncated SVD effectively only has a few discrete usable values for the regularization parameter γ . All linear filters ignore the specific structure of the data g^ε .

Nonlinear Regularization methods

In truly nonlinear regularization methods the operator T_γ has weights $w_{\gamma,i}(g^\varepsilon)$ that may change with the actual data g^ε . Two of these algorithms were tested successfully for their use in our task.

3.2 Nonlinear filtered SVD

The simplest nonlinear method is probably the filtered SVD using hard thresholding as defined by

$$w_{\gamma,i}(g^\varepsilon) = \begin{cases} 1 & ; \text{ if } |\langle g^\varepsilon | v_i \rangle| \geq \gamma \\ 0 & ; \text{ otherwise} \end{cases} .$$

If the noise coefficients $\langle z | v_i \rangle$ in the orthonormal basis $V = (v_i)$ are approximately equally distributed, than

$$\mathbb{E}(|\langle z | v_i \rangle|^2) = \frac{1}{M} \|z\|^2 \leq \frac{\varepsilon^2 \|g^\varepsilon\|^2}{M} .$$

It follows, that coefficients corrupted by noise are most likely cut out if we choose

$$\gamma > \frac{3\varepsilon \|g^\varepsilon\|}{\sqrt{M}} .$$

For an illustration see Figure 6b. Choosing γ much larger than $\frac{3\varepsilon \|g^\varepsilon\|}{\sqrt{M}}$ induces too high a regularization error. However, for most cases thresholded SVD just replicates the results of a truncated SVD in practice. But thresholded SVD regularization works especially well on data, which have their energy concentrated at some intermediate singular components (like the u_i with $i \in \{5, \dots, 8\}$ in our case) that can not be reconstructed with standard linear methods at all.

3.3 Conjugate Gradient Regularization

An alternative approach is to use data dependent functions instead of the singular functions to approximate the solution. This is done in conjugate gradient (CG) methods. Like Tikhonov regularization CG methods find the solution via some optimization problem and thus avoids computing singular vectors.

However, unlike Tikhonov regularization, the solution is not defined as an minimizing element of a residual plus penalty term. Instead finitely many (k) steps of an iterative CG minimization of the plain residual

$$\min \|Af - g^\varepsilon\|_2^2$$

are performed until the residual satisfies for the first time Morozov's discrepancy principle

$$\|Af_k - g^\varepsilon\|_2 \leq \tau\varepsilon\|g^\varepsilon\| \leq \|Af_{k-1} - g^\varepsilon\|_2 \quad \text{for some } \tau \in (1, 2] .$$

CG starting at f_0 effectively minimizes the residual over the subspace

$$f_0 + \text{span}\{(A^*A)^j r_0 \mid j = 0, \dots, k-1; r_0 := A^*(Af_0 - g^\varepsilon)\} ,$$

called the Krylov-space K^k . It is determined by properties of A , the actual data g^ε and the initial guess f_0 .

The k -dimensional Krylov-space will in general be close in some sense to the subspace spanned by the k singular vectors with the largest singular values, but Krylov-space is usually better adapted to the data than some data unrelated subspace spanned by the first singular vectors only.

Conjugate Gradient Algorithm

The basic implementation of a CG algorithm for minimizing $J(f) = \|Af - g^\varepsilon\|_Y^2$ is as follows

1. a) From data $g^\varepsilon = Af + z$, a collection of such data or a priori knowledge of the problem estimate the relative error level

$$\varepsilon \geq \mathbb{E}(\|z\|_Y) / \|g^\varepsilon\|_Y .$$

- b) Choose $\tau > 1$ according to your confidence in this estimate (significantly larger than 1 if there is a fair chance that $\|z\|_Y > \varepsilon\|g^\varepsilon\|$ may be true for certain data).

2. a) Find a good starting point f_0 (or choose $f_0 := 0$ for simplicity) .

- b) Initialize the gradient vector r_0 with

$$r_0 := \nabla J(f_0) = A^*(Af_0 - g^\varepsilon) .$$

and set the descend direction $d_0 := -r_0$ and $k := 0$.

3. Loop ($k \rightarrow k + 1$) while the residual satisfies $\|Af_k - g^\varepsilon\|_Y > \tau\varepsilon\|g^\varepsilon\|$

$$f_{k+1} := f_k + \alpha_k d_k \quad \text{with} \quad \alpha_k := \frac{\|d_k\|_X^2}{\|Ad_k\|_Y^2} \quad \left(= \frac{\|d_k\|_X^2}{\langle d_k | A^* Ad_k \rangle_X} \right)$$

$$r_{k+1} := \nabla T(f_{k+1}) \quad (= r_k + \alpha_k A^* Ad_k)$$

$$d_{k+1} := -r_{k+1} + \beta_k d_k \quad \text{with} \quad \beta_k := \frac{\|r_{k+1}\|_X^2}{\|r_k\|_X^2}$$

The regularized k -step CG-solution is defined as $f_\gamma^\varepsilon := f_k$ with regularization parameters $\gamma = \tau \cdot \varepsilon$ and $k(\gamma)$.

It is noteworthy that for larger or real time problems CG has the additional advantage to avoid the explicit solution of linear systems and may exploit potential sparsity in the matrix A . An extended analysis of the method and its regularization properties can be found in [Lou89, Han95].

3.4 Data Error estimates

Regularization methods, in particular the nonlinear ones, depend strongly on a good estimate for the data error $\mathbb{E}(\|z\|) = \varepsilon\|g^\varepsilon\|$. Fortunately in this inverse imbalance reconstruction we can have many more data dimensions than dimensions to reconstruct ($K \gg L$) therefore

$$\langle Af | v_i \rangle = 0 \quad \text{for all} \quad i = L + 1, \dots, K.$$

Hence we know

$$\langle g^\varepsilon | v_i \rangle = \langle z | v_i \rangle \quad \text{for all} \quad i > L.$$

Thus a direct noise level estimate adaptively computable from actual measured data is available via

$$\varepsilon^2 := \mathbb{E}(\|z\|_2^2) / \|g^\varepsilon\|^2 \simeq \frac{M}{\|g^\varepsilon\|^2} \mathbb{E}(|\langle z | v_i \rangle|^2) \simeq \frac{M}{(M - L)\|g^\varepsilon\|^2} \sum_{i=L+1}^M |\langle g^\varepsilon | v_i \rangle|^2$$

assuming the noise energy is almost equally distributed in the orthonormal basis of singular vectors v_i . Compared with estimates obtained from many realizations of the measurement or a priori information or guesses about the quality of the measurement the adaptive estimate from a single dataset has many practical and theoretical advantages.

Figure 7a shows 30 realizations of a simulation, their average and the quotient of average and each realization, suggesting a local error of about 10%.

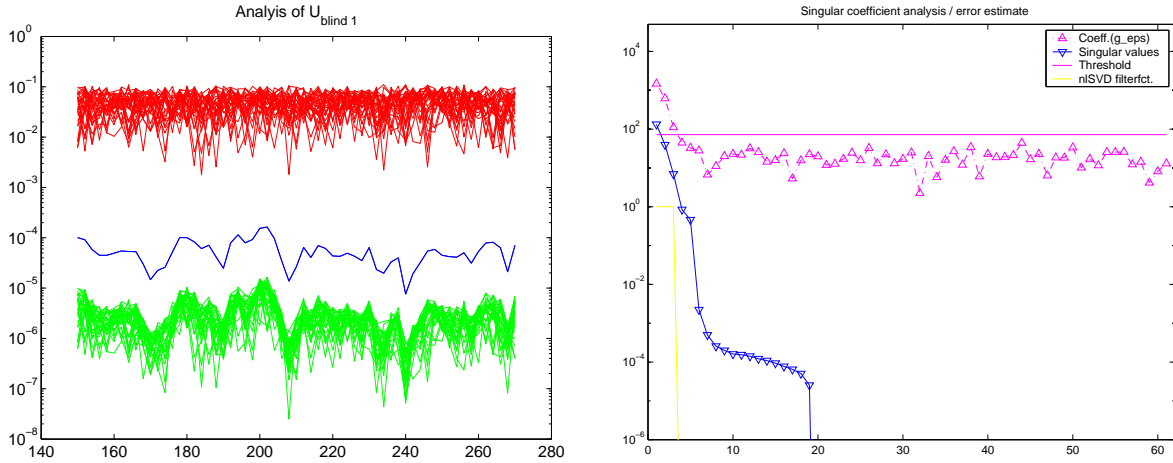


Figure 7: Error estimates from many realizations (left) may be much more expensive and less reliable for a specific data set than the adaptive estimate (right 3 times err est. threshold used with nonlinear SVD) computed from that single data set.

Figure 7b illustrates the noise based threshold used with the thresholded nonlinear SVD. It was obtained from the SVD coefficients of a single measurement g^ε as described above.

4 Numerical results

This section presents numerical results obtained from simulated data for 20 possible imbalance locations and 61 sampled frequencies. The following cases will be considered.

1. A numerical test case
2. A deformation of the axis of parabolic shape (bend)
3. A wave like deformation of the axis (wave)
4. A complex composite imbalance distribution
5. A point imbalance

4.1 Explanation of figures

The images in the following sections show the following

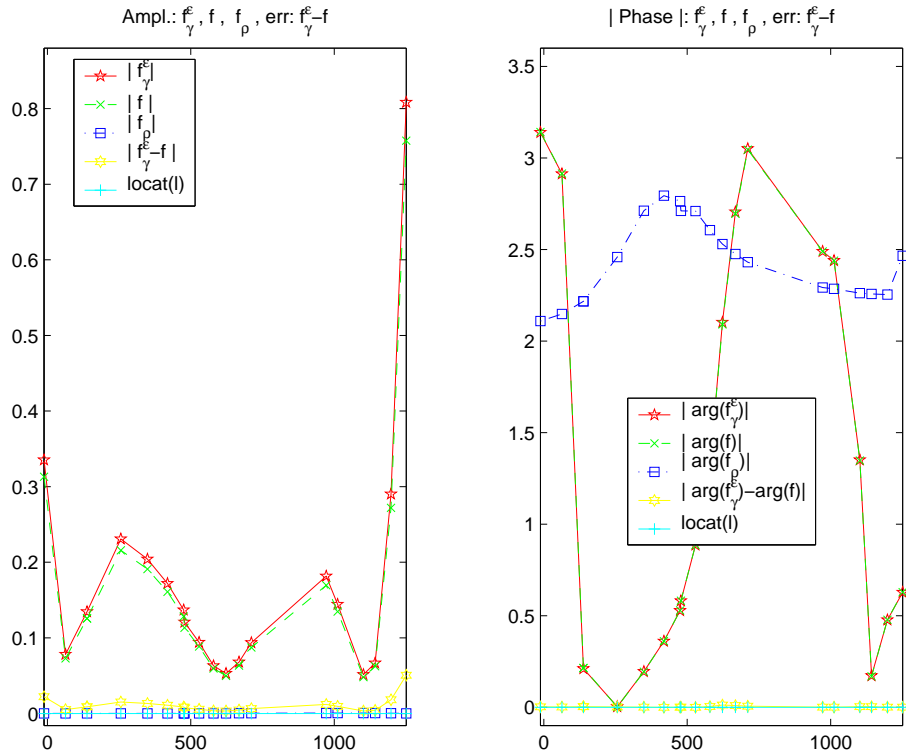
Left Amplitude of the true solution along the rotor axis as well as the CG reconstruction f_γ^ϵ and a truncated SVD reconstruction f_ρ for comparison and the error of the CG reconstruction. Further the locations of possible imbalances are indicated.

Right The same for the phase. Since phase π and $-\pi$ are equivalent the absolute value of the phase is shown in order to suppress irritating oscillations when the phase is close to $\pm\pi$.

4.2 Numerical test case

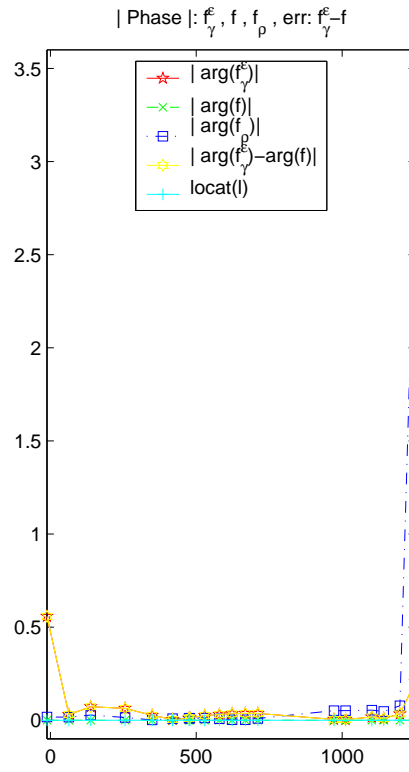
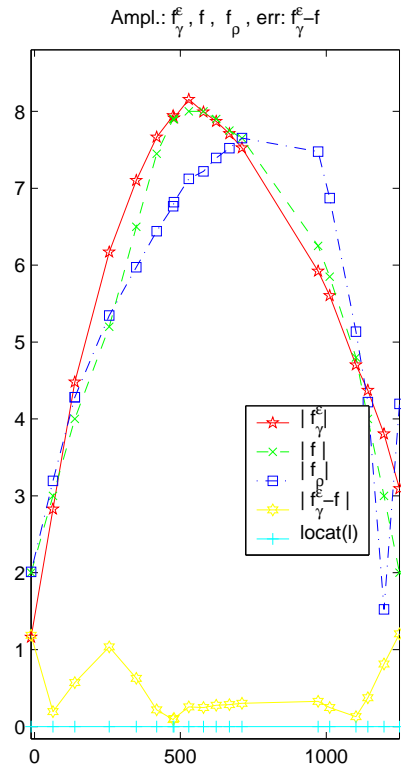
In a numerical blind test case, the challenge to reconstruct singular functions of medium order, e.g. $i = 4, 7$ from given noisy data was posed.

By its definition the standard truncated SVD must fail this test. So did all the considered linear algorithms (e.g. Tikhonov, Landweber). Only the nonlinear thresholded SVD and conjugate gradient methods performed well on this test.



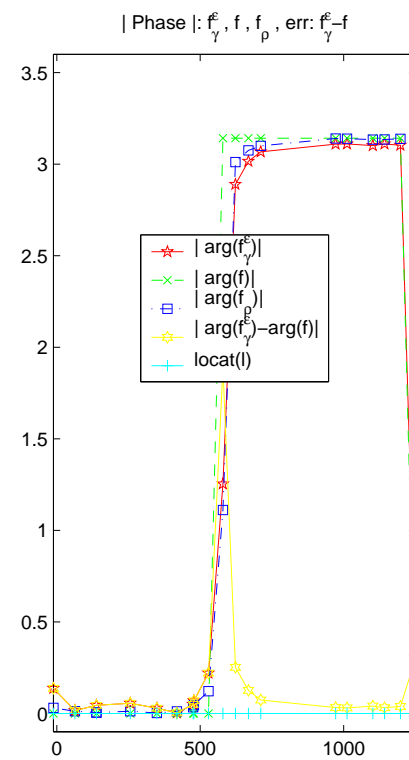
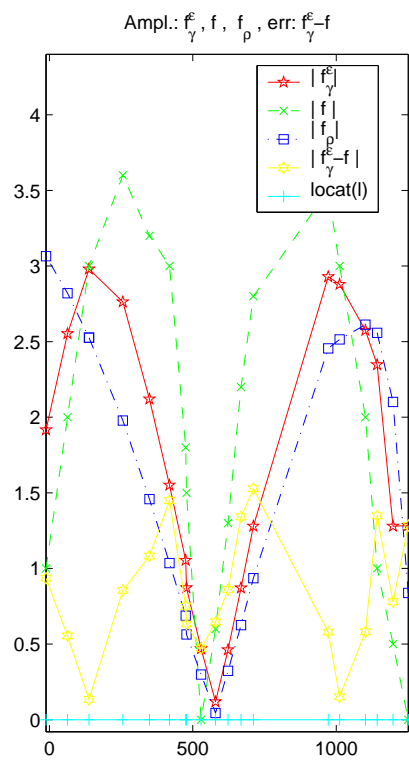
4.3 Bend deformation

The bend can be reconstructed very well, even by the standard truncated SVD, because the coefficient energy in a singular value expansion of the bend deformation is concentrated at the stable singular vectors. Truncated SVD and CG regularization with optimal regularization parameters yield very similar results.



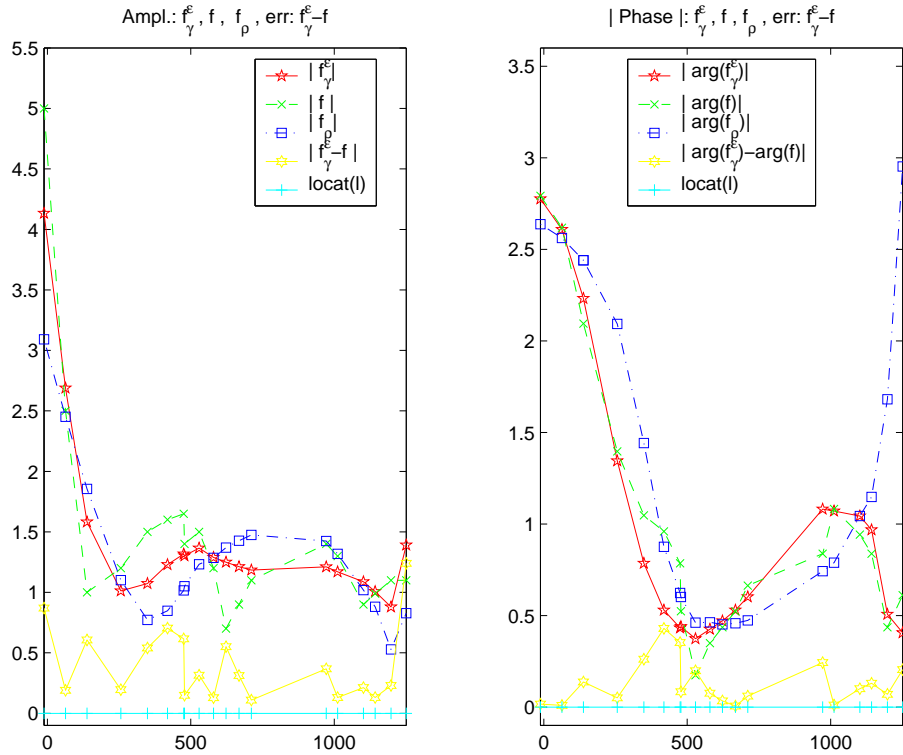
4.4 Wave deformation

For the wave deformation the situation is similar to the bend.



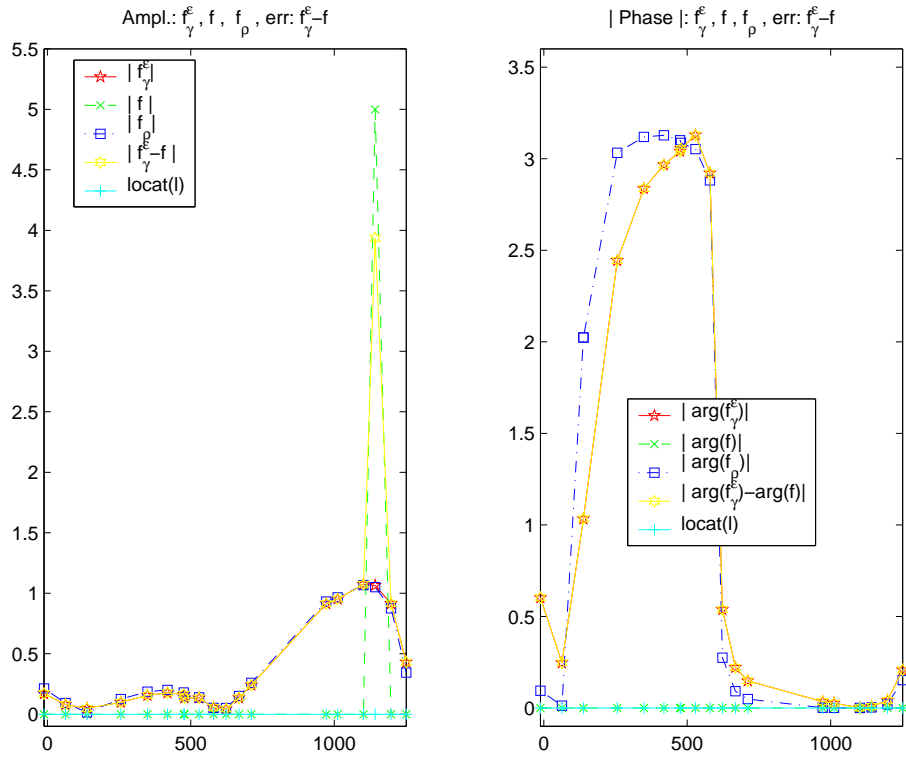
4.5 Complex imbalance

The complex situation has a distributed pattern of imbalances under various angles. The coefficient energy in the SVD is not so strongly concentrated at the most stable singular values. Advantages of the nonlinear reconstruction become apparent.



4.6 Point imbalance

Point imbalances are very hard to reconstruct. This can be understood from the distribution of the coefficient energy which is of the same order of magnitude for all singular vectors. Because many relevant coefficients of the perfect data are obscured by noise several orders of magnitude stronger, a large share of the point imbalance can not be recovered.



4.7 On coarse scale localization of point imbalances

The direct reconstruction of point imbalances turned out to be very difficult at realistic noise levels. This is mainly due to large coefficients of point imbalances related to singular vector with extremely small singular values in the singular value decomposition of these imbalances, cf. Figure 8 and 9.

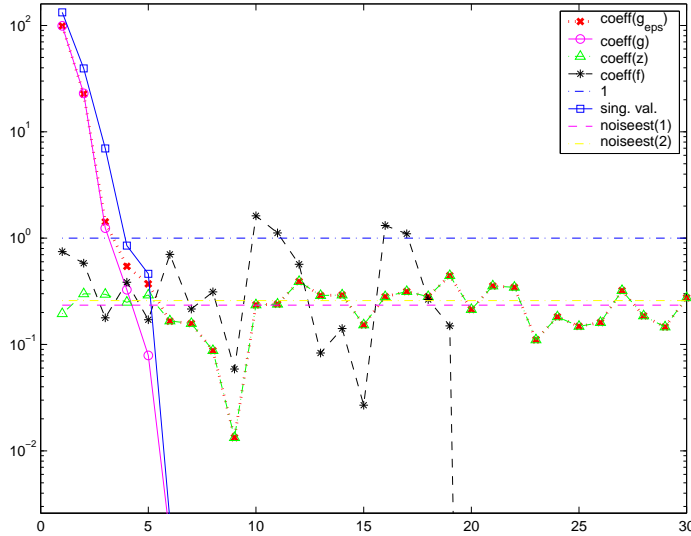


Figure 8: Singular value decomposition of solution f (point imbalance in midpoint position), data $g = Af$, noisy data $g^\epsilon = Af + z$, error estimate and singular values.

From the analysis it becomes clear, that a reliable direct identification of point imbalances is impossible, even if the model were perfectly valid and data with a relative noise of only say 0.01% were available.

4.8 Nonlinear functionals for coarse scale location

Therefore strategies to localize point imbalances on a coarser scale were developed.

These strategies are based on a 4 step CG reconstruction of the imbalance and a correlation of the absolute value of the reconstructed imbalance with either a suitably weighted characteristic function of some engine compartment or a smooth approximation of such a characteristic function. In our study a localization with respect to a trisection of the engine in front, middle, back compartment was aimed at. The following figure shows the plain and smoothed characteristic functions and their 4-CG step reconstruction.

Despite the difficulties in reconstructing point imbalances, it turned out that almost any point imbalance can be localized on a coarse scale. This is achieved using nonlinear functionals that assign to any data one of three compartments of the high pressure system that is supposed to contain the largest share of the underlying imbalance.

The functionals used for this task are based on a set of scalar products of the amplitude of a CG regularized solution with the characteristic function of the compartment or some smoothed version of the characteristic functions. These scalar products are weighted according the proportion of energy of the respective function reconstructed

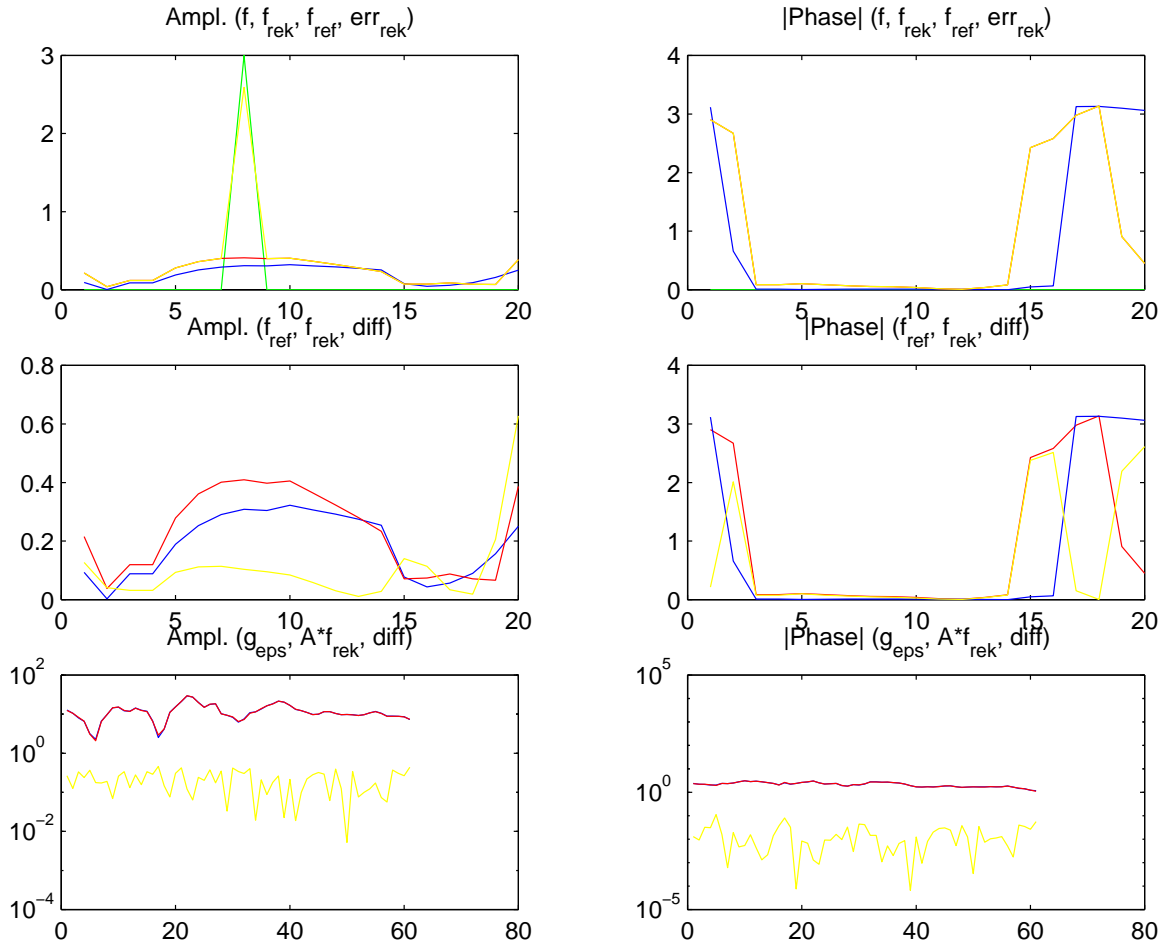


Figure 9: Analysis of a CG reconstruction of a point imbalance in a middle position. Left top: Amplitude of true solution (green) , CG (red) and Tikhonov (blue) regularized solution.

Left middle fig.: As above without the true solution (yellow: difference of the two reconst.)

Left bottom: Amplitude and amplitude error $|g^\epsilon|$ and $|g^\epsilon| - |Af_{rec}|$.

Right column: Like left column but for phase instead of amplitude of solution resp. data.

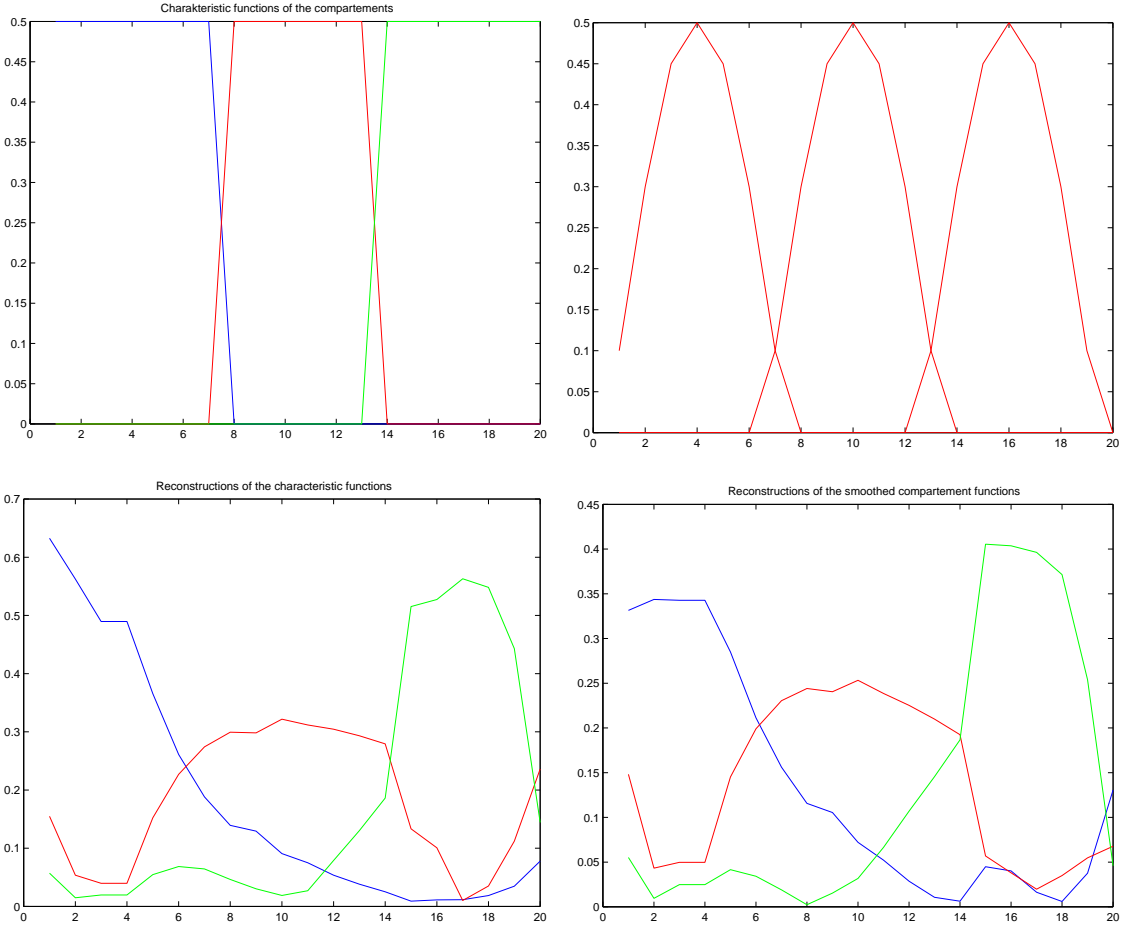


Figure 10: a)-d) Plain(a) and smoothed (b) characteristic functions of the compartments and their 4 SVD level reconstructions from noise free data for each of the functions c) and d).

from perfect data by a truncated SVD using the 4 most stable singular values. Let χ_n denote the characteristic function of the n -th compartment and $w_n = \frac{1}{\|(\chi_n)_{TSVD(4)}\|}$ the weight used to balance size effects and difficulty in reconstructing different compartments. Therefore the quantities

$$F_n(g^\varepsilon) = \langle |f_{CG}^\varepsilon| | w_n \chi_n \rangle$$

can be computed. We then chose the compartment related to χ_n as location of the imbalance causing g^ε if $F_n(g^\varepsilon)$ is largest among all these functionals. At typical noise levels this procedure locates almost surely all point imbalances correctly beside those at the boundary of the compartments.

The computations indicate that coarse scale localization is still difficult when only information related to the stable singular values may be used, in particular for the

middle compartment where only half of the characteristic functions energy is captured in the reconstructed stable part. The reconstructions overlap considerably, even in the case of the better separated smoothed functions.

Nevertheless, with the help of the nonlinear functionals it was possible to assign correctly any point imbalance not near the boundary of one of three engine compartments to its section even in the presence of 10% noise in the data, by assigning the imbalance cause to that compartment with the highest correlation. For the numerical results with both original and smoothed compartment functions cf. Tab. 1.

Pos.	F front	F middle	F back
1	1/1	0.2338/0.1348	0.1696/0.1751
2	1/1	0.1148/0.0991	0.0738/0.0907
3	1/1	0.1727/0.1987	0.1314/0.1768
4	1/1	0.1727/0.1987	0.1314/0.1768
5	1/1	0.2080/0.1974	0.1232/0.1367
6	1/1	0.6254/0.5100	0.1498/0.1647
7	0.7640/0.9603	1/1	0.2880/0.3548
8	0.5121/0.6955	1/1	0.2522/0.2928
9	0.4146/0.5765	1/1	0.2391/0.2801
10	0.3036/0.4774	1/1	0.2686/0.3033
11	0.2427/0.3615	1/1	0.3181/0.3422
12	0.2577/0.3343	1/1	0.4137/0.4454
13	0.2932/0.3424	1/1	0.6136/0.6405
14	0.4331/0.4581	1/1	0.7140/0.6256
15	0.0468/0.0576	0.1038/0.1417	1/1
16	0.0416/0.0577	0.0878/0.1235	1/1
17	0.0944/0.1158	0.1202/0.1181	1/1
18	0.1383/0.1473	0.1695/0.1364	1/1
19	0.1723/0.1264	0.1994/0.1236	1/1
20	0.3954/0.1874	0.2669/0.1116	1/1

Table 1. Relative correlations strength with the compartment functionals for 20 different point imbalances (values for true char. function/ smoothed char. fct.). For the positions 7 and 14, which are at the compartment boundaries, the assignment is wrong, but with a strong vote also for the correct neighboring compartment.

The difference between using proper or smoothed characteristic can be seen to be not very significant.

4.9 Results from real data

This research project brought together previously independent groups, therefore simulations and data collection were performed for different engine types. Due to the resulting model mismatch reconstructions using real data was not yet possible. The analysis of the real data together with the quality estimates of the real data show nevertheless, that meaningful reconstructions from real data will be possible in the future, when measurements can be done on the modeled engine or a whole engine model for a turbine in the measured configuration becomes available.

5 Conclusions

5.1 Summary

Theoretical and numerical evidence for the possibility to reconstruct the imbalance distribution in an aircraft engine turbine from measurements of vibrations on the casing was presented. Nonlinear regularization techniques, in particular conjugate gradient (CG) and possibly thresholded singular value decomposition give the most convincing results for more demanding cases in numerical simulations.

The quality of the available real measurement data will be sufficient to reconstruct slowly varying imbalance distributions like a bend or wave deformation very well. A perfect localization of point imbalances will not be possible with available algorithms even if the data quality could be much improved. This is due to the energy distribution of point sources in the singular vector basis and the strong ill-posedness of the problem. Nevertheless a localization on a coarse scale is feasible in simulations using nonlinear functionals even at poorer data quality than available in real measurements. Using similar functionals to identify typical imbalance distributions caused while assembling the engine parts, it should be possible to improve the quality of the product and monitor any changes in the imbalance distribution over the lifespan of the engine.

Meaningful reconstructions from real data will be produced in the near future when matching measurement and numerical simulation configurations are available.

5.2 Open Problems

The research poses a number of further interesting questions about the design of the optimal measurement process, the robustness of the reconstruction with respect to modeling error and applications to related problems in rotordynamics like gas turbines and generators in power plants.

Other directions for further research involve nonlinear inverse problems. It would be desirable to reconstruct the imbalance distribution also for older engines. These do not have once-per-revolution probes, a fact which renders the phase measurement impossible. Thus the demanding nonlinear task to identify f from

$$a^\varepsilon = |g^\varepsilon| = |Af| + z$$

arises.

References

- [DMR99] DICKEN, V.; MAASS, P. and REINHARDT, F.: Abschliessender technischer Bericht zum BMW Rolls-Royce Projekt: *Inverse Unwuchtbestimmung*, Univ. Bremen, Aug. 1999.
- [FGHL97] R.D.FIERRO, G.H.GOLUB, P.C.HANSEN and D.P.O'LEARY *Regularization by Truncated Total Least Squares* SIAM J.SCI.COMPUT., Society for Industrial and Applied Mathematics Vol.18, No.4, pp.1223-1241, July 1997.
- [Han95] HANKE, M.: *Conjugate Gradient Type Methods for Ill-Posed Problems*, Pitman Research Notes in Mathematics, Longman House, Harlow, Essex, 1995.
- [Lou89] LOUIS, A.K.: *Inverse und schlecht gestellte Probleme*, Teubner Verlag, Stuttgart 1989.
- [GP75] GASCH, R.; PFÜTZNER, H. *Rotordynamik*, Springer-Verlag, Berlin 1975.
- [Pe00] PETERS, D.: *Inverse Rekonstruktion von Rotorunwuchtverteilungen auf der Basis gemessener Schwingungsdaten* Diploma thesis, Rolls-Royce Germany GmbH + TU Berlin, Jan. 2000.
- [Ro00] ROTHER, J.: *Comparison of Wavelet- and Fourier presentment for signal analysis of aircraft engines* Diploma thesis, Rolls-Royce Germany GmbH + TU Berlin, Jan. 2000.
- [Wi00] WITTE, H.: *Online-monitoring for aircraft engines - development and application*, Aims-Symposium Garmisch-Partenkirchen, May 2000.